Saving Pt-Catalyzed PEM Fuel Cells from CO Poisoning by Getting COPROX to Work!

Debra R. Rolison,[1,] Travis G. Novak,[1] Paul A. DeSario,[1,*] Todd H. Brintlinger,[2] Ryan H. DeBlock,[1] and Jeffrey W. Long[1]*

[1] Surface Chemistry Branch, U.S. Naval Research Laboratory, Washington, D.C. 20375, United States

[2] Materials & Sensors Branch, U.S. Naval Research Laboratory, Washington, D.C. 20375, United States

*Corresponding Authors: debra.rolison@nrl.navy.mil; paul.desario@nrl.navy.mil

Abstract: We design ultraporous metal nanoparticle–modified oxide aerogels as architected platforms that impose size comparability of the networked, covalently bonded oxide nanoparticles (NPs) and the catalytic NPs supported thereon. This arrangement permits a degree of physical and chemical interfacial intimacy uncommon in heterogeneous catalysis. We find that such high contact intimacy for photodeposited copper nanoparticles on reducing oxide aerogels such as ceria stabilizes Cu in its more catalytically active, low-valent (0 or +1) state, even poising sufficient Cu(0) in the supported particle for plasmonic character to persist even under oxidizing conditions. We previously evaluated the selectivity and activity of this architected catalyst and a related aerogel, $Cu/Gd_xCe_{1-x}O_2$, for preferential oxidation of CO (COPROX) in H_2 feedstreams, finding that $Cu/Gd_xCe_{1-x}O_2$ outperformed Cu/CeO_2 when H_2 and H_2O were present in the feedstream. Here, we explore a series of $Cu/Gd_xCe_{1-x}O_2$ aerogels and evaluate their performance for dry CO oxidation. The surface area of the aerogels increases as Gd content increases, explaining the improved performance of $Cu/Gd_xCe_{1-x}O_2$ under humid COPROX conditions where transport is known to be a limiting factor, but catalytic activity towards CO oxidation decreases under dry conditions. These results reflect an important trade-off between improved transport but reduced fundamental redox capacity with Gd substitution into CeO_2 aerogels.

Keywords: Catalysis, aerogel, oxygen vacancy, oxidation, mesoporous

Introduction

Transition metals supported on or embedded in a CeO_2 support provide exceptional catalytic properties for many reactions relevant for fuels production/purification and environmental remediation, including preferential oxidation of CO (COPROX), water–gas shift (WGS), CO_2 hydrogenation, and NO_x reduction.[1] An aerogel expression of CeO_2 provides an excellent platform for catalysis because this morphology provides a high-surface area and an interconnected pore network, exposes abundant active sites, and maximizes interfacial intimacy between the metal and oxide support.

Oxygen vacancies (O_{vac}) in the CeO_2 play an important role in many oxidation reactions, often serving as defect sites for adsorption and activation of reactant species, e.g., adsorbed H_2O on CeO_2 dissociates at oxygen vacancies to form surface hydroxyls.[2] Activation of the reactants is not always the rate-limiting step; DFT calculations reveal an inverse relationship between the activity of CeO_2 for WGS and its oxygen-vacancy density.[3] In cases where metal cations with <4+ valency are substituted into the CeO_2 lattice to generate additional oxygen vacancies, the catalyst morphology may be affected, making it difficult to deconvolve the effects.

In this work we assess the impact of Gd-substitution on oxygen-vacancy concentration and CeO_2 aerogel morphology. We evaluate the CO oxidation activity of Gd(III)-substituted and native CeO_2 aerogels after photodepositing 5 wt% Cu on the aerogel network. We find that as the Gd content increases in $Gd_xCe_{1-x}O_2$, so does the surface area of the aerogel and its oxygen-vacancy concentration. However, the intrinsic activity of $Cu/Gd_xCe_{1-x}O_2$ for CO oxidation decreases.

Results and Discussion

Aerogels were synthesized using a previously reported sol–gel method.[4–7] For CeO_2, 2.39 g of $CeCl_3 \cdot 7H_2O$ was dissolved in 10 g of anhydrous

methanol, followed by adding 6 g of propylene oxide, vigorously stirring for 20 min, then leaving the sol to gel overnight. For Gd(III)-substituted CeO_2 (GCO) aerogels, 5, 10, and 20 mol% of $GdCl_3 \cdot 6H_2O$ were substituted for corresponding amounts of $CeCl_3 \cdot 7H_2O$ to form gels designated 5GCO, 10GCO, and 20GCO, respectively. The wet gels were rinsed several times in isopropanol, then acetone, then supercritically dried in CO_2. For CO oxidation testing, 5 wt% Cu was photodeposited by mixing 200 mg of ground aerogel with 38 mg of $Cu(NO_3)_2 \cdot H_2O$, adjusting the dispersion pH to 9.5±0.1 with NaOH, and irradiating for 48 h using a 500 W Xe arc lamp. This protocol yields well-dispersed, aerogel-supported nanoparticulate Cu in which the Cu is stabilized primarily in its low-valent ($Cu^{0/1+}$) state. The wetting/drying steps necessary to photodeposit Cu from aqueous media does not affect the morphology of the calcined aerogel.[5,7]

Figure 1 summarizes the impact of Gd(III) substitution on CeO_2 morphology, as measured by Brunauer–Emmett–Teller (BET) surface area. After being supercritically dried, all CeO_2 and GCO aerogels show essentially identical surface areas, between 299.6 and 302.8 m^2/g, differences well within typical experimental error. The Gd precursor itself is highly amenable to gel formation, previously reported to form monolithic Gd_2O_3 aerogels with high surface area through a similar synthesis route,[8] so it does not adversely affect surface area.

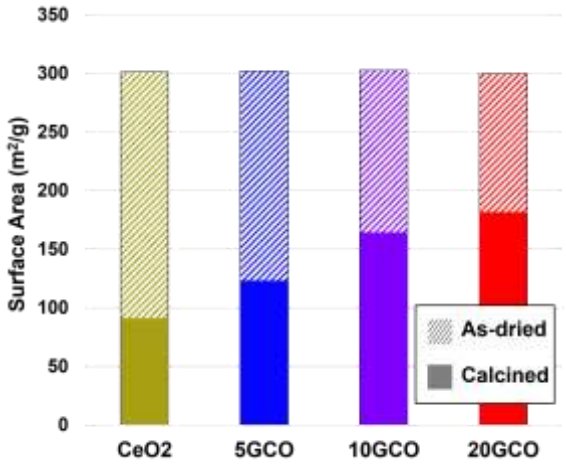

Figure 1 | BET surface area of dried (shaded) and 500 °C-calcined (solid) aerogels.

As Gd content increases, the aerogels retain more surface area after calcination at 500 °C (Figure 1). All aerogels inevitably lose surface area during calcination as crystallite growth reduces porosity, but Gd substitution slows crystallite growth in CeO_2.[9] As a result, the surface area of 20GCO (181.6 m^2/g) is nearly double that of the native CeO_2 aerogel (91.1 m^2/g).

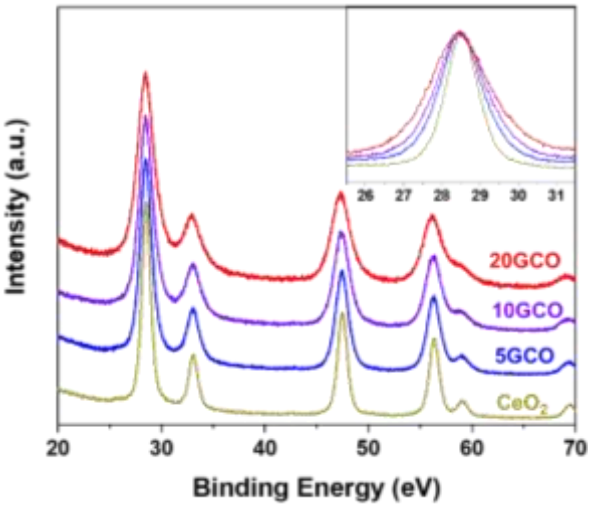

Figure 2 | XRD patterns of CeO_2 and GCO aerogels, with inset showing broadening of the ⟨111⟩ peak as the mol% of Gd(II) substituted into CeO_2 aerogel increases.

Changes to the crystallite size upon Gd-substitution are corroborated by X-ray diffraction (XRD) analysis (Figure 2). All diffraction peaks correspond to the CeO_2 fluorite structure, indicating that even at 20 mol%, Gd does not form a discrete Gd_2O_3 phase. Increasing Gd content results in peak broadening (Figure 2, inset), a product of smaller crystallite size and/or lattice strain as Gd(III) substitutes in Ce(IV) sites. Crystallite size, estimated using the Scherrer equation, decreases from 8.9 nm in CeO_2 aerogel to 4.9 nm in 20GCO. The primary ⟨111⟩ peak also slightly shifts; the calculated lattice spacing expands from 3.132 Å for CeO_2 to 3.138 Å for 20GCO.

We use X-ray photoelectron spectroscopy (XPS) to probe the changes in chemical states between different compositions of aerogels (Figure 3). In the O1s region, the lower binding energy peak (O_a) is assigned to lattice oxygen in stoichiometric CeO_2, while the higher binding

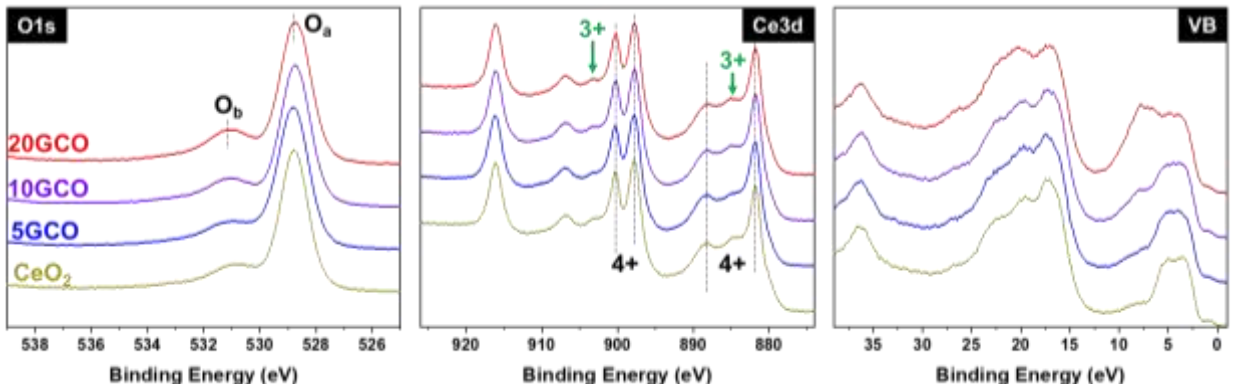

Figure 3 | XPS of the O1s, Ce3d, and VB regions of CeO_2 and GCO aerogels.

energy peak (O_b) originates from O or OH coordinated with Ce^{3+}.[10] The intensity of the O_b peak increases with increasing Gd mol%, and the presence of increased oxygen vacancies is also evident in the slight increase in Ce^{3+} peaks in the Ce3d region. The valence band (VB) region further confirms the presence of Gd by the appearance of a progressively bigger shoulder at ~9 eV as Gd content increases, a binding energy characteristic of a Gd–O chemical state.[11]

We then photodeposited 5 wt% Cu over the four aerogel supports and evaluated their performance for the CO oxidation reaction. Oxidation of CO is often used as a benchmark reaction and is generally thought to proceed via the Mars van Krevelen (MvK) mechanism, where adsorbed CO is oxidized by a lattice oxygen, and the resulting oxygen vacancy is healed to restart the catalytic cycle.[12] For the active site to turnover, it is not the presence of oxygen vacancies prior to CO exposure that is beneficial, but rather the ability of the CeO_2 to cycle between 3+/4+ states as vacancies are generated and healed. A persistent oxygen vacancy – i.e., one that does not heal in the presence of oxygen – should adversely affect catalysis if the MvK mechanism is dominant.

Although $5Cu/CeO_2$ and 5Cu/5GCO show similar CO oxidation light-off curves (Figure 4), the impact of fixed vacancies becomes more pronounced at higher Gd loading. 5Cu/20GCO, which has the highest oxygen vacancy content, is by far the least active aerogel across the measured temperature range. The activity of 5Cu/10GCO decreases at lower temperatures, but eventually reaches approximately the same activity of $5Cu/CeO_2$ at 150 °C. It is possible that as conversion percentages become higher, the greater surface area of 10GCO is better able to ease kinetic limitations. Alternatively, a non–MvK mechanism, such as one invoking Cu–Ce dual-site adsorption,[13] may become favorable at higher temperatures. Overall, these results indicate that the increased surface area and oxygen-vacancy concentration induced by Gd(III)-substitution do not positively impact low-temperature CO oxidation.

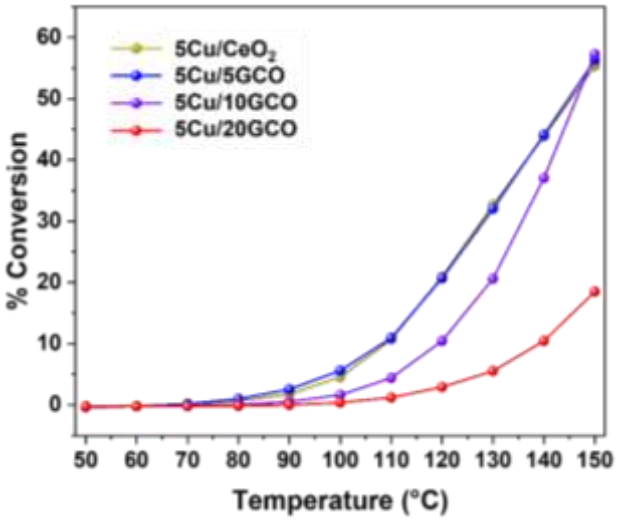

Figure 4 | CO oxidation light-off curves for 5 wt.% Cu photodeposited over CeO_2 and GCO aerogel supports.

Summary

We demonstrate a tradeoff between the surface area/oxygen vacancy concentration and CO oxidation performance when Gd(III) is substituted into the lattice of CeO_2 aerogels. The results hold important implications for catalyst design, where the specific reaction limitations

should be considered. In reactions that have few transport limitations and facile activation of reactants, such as the case with dry CO oxidation, maximizing the number of sites available for 3+/4+ redox promotes the best low-temperature activity. However, our previous work with the COPROX reaction finds that in the presence of water, Gd-substituted CeO_2 aerogel, with its greater surface area and ability to activate H_2O at oxygen vacancy sites, affords superior activity.[5]

Acknowledgments

This work was supported by the Office of Naval Research. T.G.N. and R.H.D. were NRL-NRC postdoctoral associates from 2020–2023.

References

1. Konsolakis, M. The Role of Copper–Ceria Interactions in Catalysis Science: Recent Theoretical and Experimental Advances. *Appl. Catal. B* **2016**, *198*, 49–66.

2. Yang, Z.; Wang, Q.; Wei, S.; Ma, D.; Sun, Q. The Effect of Environment on the Reaction of Water on the Ceria(111) Surface: A DFT+U Study. *J. Phys. Chem. C* **2010**, *114*, 14891–14899.

3. Vecchietti, J.; Bonivardi, A.; Xu, W.; Stacchiola, D.; Delgado, J.J.; Calatayud, M.; Collins, S.E. Understanding the Role of Oxygen Vacancies in the Water Gas Shift Reaction on Ceria-Supported Platinum Catalysts. *ACS Catal.* **2014**, *4*, 2088–2096.

4. Novak, T.G.; DeSario, P.A.; Johannes, M.D.; Brintlinger, T.H.; DeBlock, R.H.; Long, J.W.; Chervin, C.N.; Stroud, R.M.; Rolison, D.R. CeO_2 Aerogel-Induced Resilience of Catalytic $Ni(OH)_2$ under Oxidizing Conditions. *Chem. Mater.* **2022**, *34*, 5644–5653.

5. Novak, T.G.; DeSario, P.A.; Brintlinger, T.H.; DeBlock, R.H.; Long, J.W.; Rolison, D.R. Cu/CeO_2 and Cu/Gd-Substituted CeO_2 Aerogels as Active, Selective, and Stable COPROX Catalysts. *ACS Sustain. Chem. Eng.* **2023**, *11*, 2853–2860.

6. Novak, T.G.; Balow, R.B.; Buck, M.R.; Rolison, D.R.; DeSario, P.A. Dark and UV-Enhanced Degradation of Dimethyl Methylphosphonate on Mesoporous CeO_2 Aerogels. *ACS Appl. Nano Mater.* **2023**, *6*, 3075–3084.

7. Pitman, C.L.; Pennington, A.M.; Brintlinger, T.H.; Barlow, D.E.; Esparraguera, L.F.; Stroud, R.M.; Pietron, J.J.; DeSario, P.A.; Rolison, D.R. Stabilization of Reduced Copper on Ceria Aerogels for CO Oxidation. *Nanoscale Adv.* **2020**, *2*, 4547–4556.

8. Zhang, H.D.; Li, B.; Zheng, Q.X.; Jiang, M.H.; Tao, X.T. Synthesis and Characterization of Monolithic Gd_2O_3 Aerogels. *J. Non-Cryst. Solids* **2008**, *354*, 4089–4093.

9. Inaba, H.; Nakajima, T.; Tagawa, H. Sintering Behaviors of Ceria and Gadolinia-Doped Ceria. *Solid State Ionics* **1998**, *106*, 263–268.

10. Sohn, H.; Celik, G.; Gunduz, S.; Dogu, D.; Zhang, S.; Shan, J.; Tao, F.F.; Ozkan, U.S. Oxygen Mobility in Pre-Reduced Nano- and Macro-Ceria with Co Loading: An AP-XPS, In-Situ DRIFTS and TPR Study. *Catal. Lett.* **2017**, *147*, 2863–2876.

11. Zatsepin, D.A.; Boukhvalov, D.W.; Zatsepin, A.F.; Kuznetsova, Y.A.; Mashkovtsev, M.A.; Rychkov, V.N.; Shur, V.Y.; Esin, A.A.; Kurmaev, E.Z. Electronic Structure, Charge Transfer, and Intrinsic Luminescence of Gadolinium Oxide Nanoparticles: Experiment and Theory. *Appl. Surf. Sci.* **2018**, *436*, 697–707.

12. Sun, Y.; Li, C.; Djerdj, I.; Khalid, O.; Cop, P.; Sann, J.; Weber, T.; Werner, S.; Turke, K.; Guo, Y.; Smarsly, B.M.; Over, H. Oxygen Storage Capacity versus Catalytic Activity of Ceria–Zirconia Solid Solutions in CO and HCl Oxidation. *Catal. Sci. Technol.* **2019**, *9*, 2163–2172.

13. Ji, W.; Chen, X.; Li, Q.; Lin, K.; Deng, J.; Xing, X. Insights into CO Oxidation in Cu/CeO_2 Catalysts: O_2 Activation at the Dual-Interfacial Sites. *Eur. J. Inorg. Chem.* **2023**, *26*, e202200656.